Metals and Materials International (2019) 25:912–917
https://doi.org/10.1007/s12540-019-00258-7

Back-Stress Effect on the Mechanical Strength of TWIP-IF Steels Layered Sheet

Jung Gi Kim[1] · Min Ji Jang[1] · Hyung Keun Park[1] · Kwang-Geun Chin[2] · Sunghak Lee[1] · Hyoung Seop Kim[1,2,3]

Received: 9 January 2019 / Accepted: 11 February 2019 / Published online: 19 February 2019

Abstract
Although back-stress contributes to the mechanical properties of materials, the degree of strength enhancement from back-stress is not easy to estimate. In this research, back-stress hardening of twinning-induced plasticity (TWIP) + interstitial free (IF)-layered steel sheets were estimated by implementing a non-linear combined isotropic and kinematic hardening model. High back-stress evolution occurs due to plastic strain incompatibility between a TWIP-steel core and IF-steel sheath, and the strength of TWIP + IF layered steel sheath is greater than the strength estimated by the rule-of-mixtures. A non-linear combined isotropic and kinematic hardening model was used to estimate the strength enhancement from back-stress hardening, and the simulation results were correlated with the experimental results. This result shows that the back-stress evolution in heterogeneous materials contributes to their strength, and that the non-linear combined isotropic and kinematic hardening should be included to estimate the degree of back-stress hardening.

Keywords Heterogeneous structure · Laminate materials · Back-stress · Mechanical properties · Finite element method

1 Introduction

Recently, the heterogeneity of materials has become an attractive quality when enhancing the mechanical properties of metallic materials [1]. To design a heterogeneous structure (HS) into the materials, several processing methods (e.g., surface treatment [2, 3], roll-bonding [4, 5], and powder metallurgy [6]) have been introduced. Based on these processing methods, several researchers successfully developed HS materials with layered structures [7–9], harmonic structures [10, 11], and gradient structures [2, 12]. Because plastic strain incompatibility occurs at the interfacial region due to the different properties of the hard and soft phases, geometrically necessary dislocations (GNDs) accumulate near the interface of HS materials to relieve the strain gradients [13, 14]. The accumulated GNDs interact with the mobile dislocations and provide additional strength to the HS materials.

For this reason, back-stress (σ_B) hardening, which originated from the GND accumulation at the interface, acts as an additional mechanism for strengthening the HS materials [15]. The presence of σ_B can be observed by (i) GND distributions detectable with electron backscattering diffraction (EBSD) analysis or (ii) hysteresis loops from the loading–unloading-reloading (LUR) test. Because the GND density has a linear relation with a Kernal average misorientation distribution, the GND distribution can be observed using the EBSD analysis [16]. Ma et al. observed the GND accumulation at the interface during plastic deformation of the copper/bronze laminated sheet. The EBSD analysis results show that the GND density of the interface region is greater than that of the interior region [7]. Because the dislocations are piled-up and blocked at the interface, long-range σ_B evolves because of resistance to dislocation slip in the HS materials [17]. Because the LUR test is an efficient method for investigating the Bauschinger effect, Wu et al.

Jung Gi Kim and Min Ji Jang have contributed equally to this work.

✉ Hyoung Seop Kim
hskim@postech.ac.kr

[1] Department of Materials Science and Engineering, Pohang University of Science and Technology (POSTECH), Pohang 37673, Republic of Korea

[2] Graduate Institute of Ferrous Technology, Pohang University of Science and Technology (POSTECH), Pohang 37673, Republic of Korea

[3] Center for High Entropy Alloys, Pohang University of Science and Technology (POSTECH), Pohang 37673, Republic of Korea

[18] calculated the σ_B of heterogeneous lamellar titanium by conducting a LUR test. As a result, hysteresis loops could be observed even in the first LUR cycle near the yield point due to the GND accumulation at the coarse–fine grain interface. These two results revealed that the σ_B evolves during plastic deformation of HS materials, and that the evolved σ_B contributes to the mechanical properties of metallic materials.

Although the previous reports show that σ_B evolution occurs during plastic deformation of the HS materials and that the evolved σ_B provides additional strength to the materials, the estimation of the degree of strength enhancement from the σ_B is not well represented. The Bauschinger effect was caused by springback from σ_B, which is an important issue in sheet metal forming. In order to predict and analyze springback, various analytical models have been used, such as isotropic hardening, anisotropic hardening, kinematic hardening, or combinations thereof [19–22]. Among them, the non-linear combined isotropic and kinematic hardening models showed good agreement with experimental results; therefore, they were used in this study.

In this study, the σ_B effect on the mechanical property of the twinning-induced plasticity (TWIP) + interstitial free (IF) layered steel was investigated by combining experimental and simulation approaches. To investigate the σ_B changes of the TWIP + IF layered steels during plastic deformation, LUR test was conducted with 2.5% elongation spacing in each cycle. To consider the σ_B evolution of TWIP + IF layered steel during the finite element method (FEM), combined isotropic and kinematic hardening code was added to the user subroutine in ABAQUS software. The σ_B data measured by the experimental method were used to perform simulations with higher accuracy. The simulation results are compared with the stress–strain curves from the conventional tensile test.

2 Experimental and Simulation Procedures

TWIP + IF layered steel sheets were manufactured by POSCO and the configuration of the steel layers is shown in Table 1. The stacked steel sheet was homogenized at 1200 °C for 1 h and hot rolled from 40 to 2.5 mm thickness in a 900–1100 °C temperature regime. After the hot rolling process, the sheet was cold rolled from 2.5 to 1 mm thickness and annealed at 820 °C for 30 s [23, 24].

Table 1 The volume fraction of the TWIP + IF layered steel sheets

	IF-sheath (%)	TWIP-Core (%)	IF-sheath (%)
Layer-1:6:1	12.5	75	12.5
Layer-1:2:1	25	50	25
Layer-1:1:1	33	33	33

The mechanical properties of the TWIP + IF-layered steel sheets were evaluated using tensile tests. The samples were machined to form 5 mm-gauge length plate-type sub-sized tensile specimens. The tensile test was conducted using a universal testing machine (Instron 1361, Instron Corp., Canton, MA, USA) at room temperature at a 1×10^{-3} s^{-1} strain rate. Digital image correlation (DIC; ARAMIS v 6.1, GOM Optical Measuring Techniques, Germany) was employed with a white-black speckled pattern on the surface of the tensile specimen to measure the strain during tensile deformation.

To evaluate the contribution of back-stress to the strength of the TWIP + IF layered steel sheets, a loading–unloading-reloading (LUR) test was conducted [18]. The dimensions of the LUR test specimen was the same as the conventional tensile test specimen. Each LUR cycle was divided into three steps. In the first step, 2.5% strain at a strain rate of 1×10^{-3} s^{-1} was applied to the tensile specimen. In the second step, the specimen was unloaded at a strain rate of 1×10^{-3} s^{-1} until the applied load was close to zero. In the third step, the reloading started at a strain rate of 1×10^{-3} s^{-1}. The loading–unloading cycle was repeated until elongation of the sample reached 30%.

To provide simulation results to correlate with the experimental results, FEM was conducted using ABAQUS (Ver. 6.9-EF/2, Dassault Systems, France) software. The simulation conditions set were the same conditions used in the conventional tensile and LUR tests. In addition, the user subroutine was coded to calculate the combined isotropic and kinematic hardening. In the elastic step, the trial-equivalent Von-Mises stress (σ_e^{tr}) can be calculated as follows:

$$\sigma_e^{tr} = \sqrt{\frac{1}{2}\left[\left(\sigma_{11} - \alpha_{11} - \sigma_{22} + \alpha_{22}\right)^2 + \cdots + 6\left(\left(\sigma_{12} - \alpha_{12}\right)^2 + \cdots\right)\right]}, \tag{1}$$

where σ_{ij} is a stress tensor and α_{ij} is a shift stress tensor (often called back-stress). Assuming that the infinitesimal increment in kinematic hardening is directly proportional to that in the plastic strain (ε_{ij}^p) with the proportionality constant of the kinematic hardening parameter (c), the back-stress can be expressed as follows:

$$\delta\alpha_{ij} = c \cdot \delta\varepsilon_{ij}^p. \tag{2}$$

In plastic deformation, the yield condition (f) is defined as follows:

$$f = \sigma_e^{tr} - (3G + c)\Delta p - r - \sigma_y = 0, \tag{3}$$

where G is the shear modulus, Δp is the effective plastic strain increment, r is an isotropic hardening function, and σ_y is the initial yield stress. The radial return mapping process

can be driven by the Newton–Raphson method in iterative form as follows:

$$r^{(k)} = r_t + h\Delta p^{(k)}, \tag{4}$$

$$d\Delta p = \frac{\sigma_e^{tr} - (3G + c)\Delta p^{(k)} - r^{(k)} - \sigma_y}{3G + c + h}, \tag{5}$$

$$\Delta p^{(k+1)} = \Delta p^{(k)} + d\Delta p, \tag{6}$$

where the subscript t refers to the previous time step and h is an isotropic hardening parameter.

The material tangent can be written as follows:

$$\delta\underline{\sigma} = \left[2GQ\underline{I} + \left(K - \frac{2}{3}GQ\right)\underline{I}\underline{I} + 2GR\frac{\left(\underline{\sigma}^{tr'} - \underline{\alpha}_t\right)}{\sigma_e^{tr}} \right] : \delta\underline{\varepsilon}, \tag{7}$$

$$Q = \frac{\sigma_e + c\Delta p}{\sigma_e^{tr}}, \tag{8}$$

$$R = \frac{3}{2} \cdot \frac{1}{1 + c/3G}\left(1 - \frac{3G + c}{3G + h + c} - \frac{\sigma_e}{\sigma_e^{tr}}\right), \tag{9}$$

where $\underline{I}$ is the fourth-order identity tensor, $\underline{I}$ is the second-order identity tensor, σ_e is equivalent Von-Mises stress, $\underline{\sigma}^{tr'}$ is a deviatoric trial stress tensor, and $\underline{\alpha}_t$ is the shift stress tensor at the previous time step.

3 Results and discussion

Figure 1a represents the stress–strain curves of the TWIP + IF layered steel and of monolithic steel. The strength of the layered steel sheet decreases as the volume fraction of the IF steel-sheath increases. The yield strength (σ_y) and tensile strength (σ_{TS}) of the TWIP + IF layered steel sheets are plotted in Fig. 1b to compare with the strength estimated using the simple rule-of-mixtures (ROM). The results show that both σ_y and σ_{TS} are 30–50 MPa larger than the strength estimated using the simple ROM. The extra strength in the TWIP + IF-layered steel sheet arose from the accumulation of GNDs that relieved the plastic-strain incompatibility at the interface [8]. In addition, the strength difference from the σ_B hardening also can be observed in the conventional FEM simulation result (see Fig. 2). In the conventional FEM, the

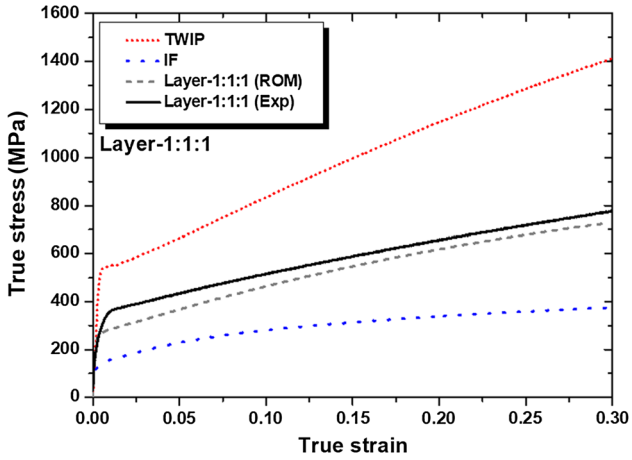

Fig. 2 True stress–strain curves of the Layer-1:1:1 from the tensile test and conventional FEM simulation

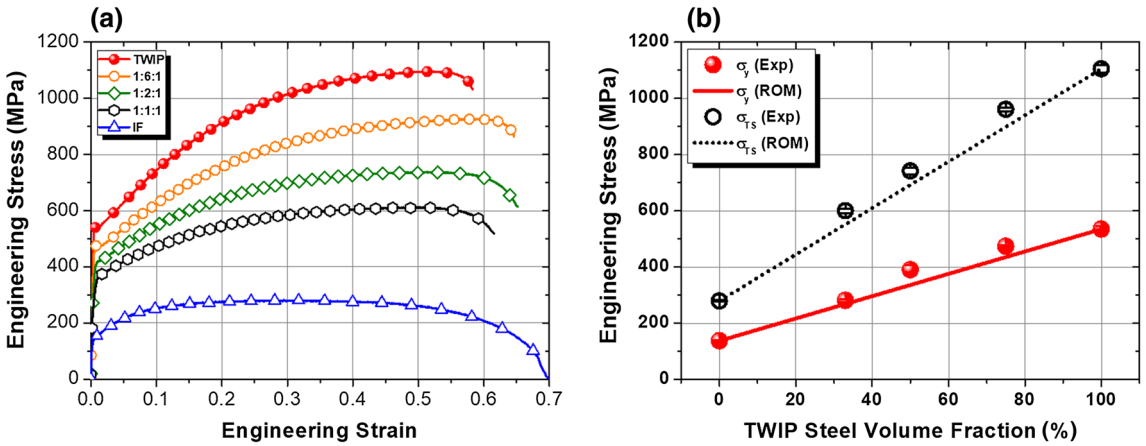

Fig. 1 **a** Engineering stress–strain curves of the TWIP, IF, and TWIP + IF layered steels. **b** The yield strength (σ_y) and tensile strength (σ_{TS}) of the TWIP + IF layered steels with increase of the TWIP steel-core volume fraction

strength is calculated according to the simple ROM of the volume fraction of parent materials [24], disregarding GND accumulation at the interface. Figure 2 represents that the extra-strength of Layer-1:1:1 originates from σ_B evolution in the early plastic deformation and that the σ_B remains during tensile deformation. In other words, although the extra-strength of the TWIP + IF layered steel originates from the σ_B evolution by GND accumulation, the conventional FEM code shows a deviation from the experimental results. Therefore, the experimental strength of the layered steel sheet is greater than the strength calculated from the conventional FEM result. Thus, the σ_B effect should be considered to increase the simulation accuracy.

To consider the σ_B contribution to the mechanical properties of materials, the σ_B of the TWIP + IF layered steel sheet was quantified by conducting LUR tests. Figure 3a shows the true stress–strain curves of the TWIP + IF layered steel sheets from the LUR test, and the hysteresis loop is seen to occur early in the plastic deformation. This hysteresis loop is induced by the deviation from the initial elastic behavior during the unloading (second) step, in which the configurations of the GNDs are partially changed by reverse strain [15]. Therefore, the accumulated GNDs contribute to the Bauschinger effect of the TWIP + IF layered steel by producing long-range back stress and the σ_B increases with strain, as represented in Fig. 3b. Because strain partitioning occurs in the elastic–plastic deformation transition region, the σ_B of the TWIP + IF layered steel sheet has already evolved in the early stage of plastic deformation. The σ_B increases as the volume fraction of IF steel-sheath decreases. According to the research conducted by Ma et al., the hardening capacity of the layer interior remains almost the same regardless of interface spacing [6]. Therefore, the influence of the interface on σ_B is the same for all three TWIP + IF layered steel sheets, and the difference in σ_B is caused by the intrinsic properties of the constituent material.

To consider the σ_B evolution of the TWIP + IF layered steel sheet in relation to the non-linear combined isotropic and kinematic hardening FEM, both the σ_B from the LUR test (Fig. 3b) and the stress–strain curves from the conventional tensile test (Fig. 1a) were used as input data for the simulation. Figure 4 presents the true stress–strain curves of the TWIP + IF-layered steel sheets from the tensile tests and from the combined isotropic and kinematic-hardening FEM simulations. Contrary to the conventional FEM simulation results in Fig. 2, the combined isotropic and kinematic hardening FEM simulation results are well correlated with the experimental results due to the addition of the σ_B term to the kinematic hardening. This result implies that the gap in strength between the experimental result and the conventional FEM simulation in Fig. 2, mainly originates

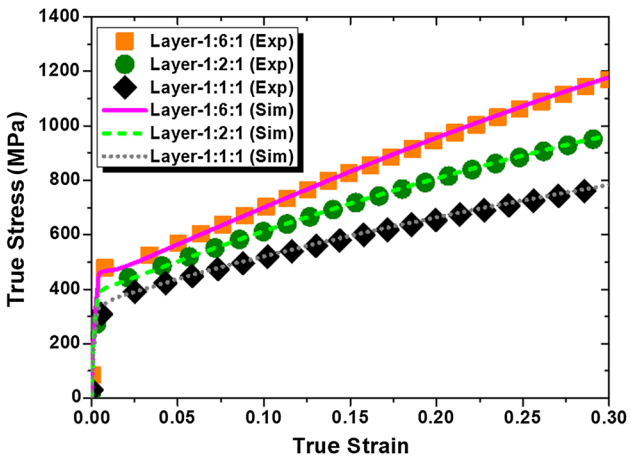

Fig. 4 True stress–strain curves of the TWIP + IF layered steels from the experiment and from the FEM simulation considering back stress

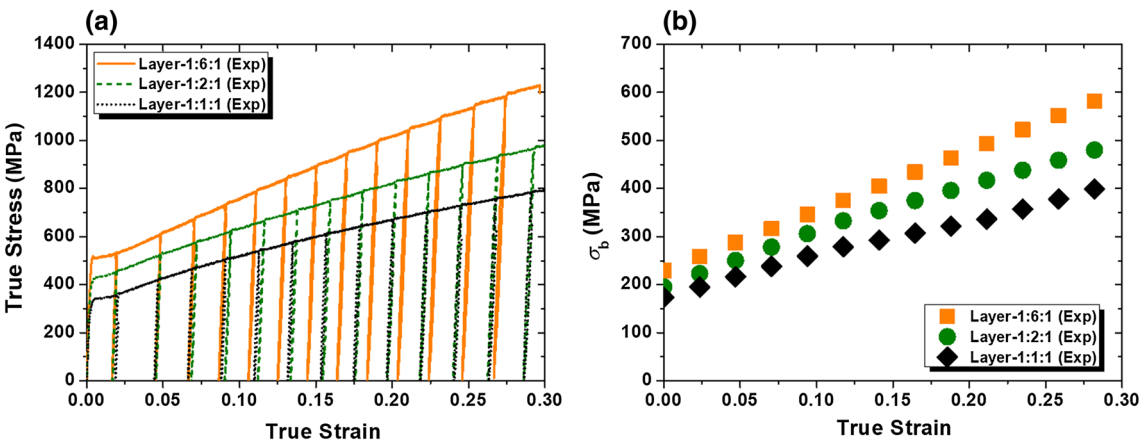

Fig. 3 **a** True stress–strain curves of the TWIP + IF layered steel sheets from the LUR test and **b** back-stress (σ_B) of the TWIP + IF layered steel sheets with increase of the true strain

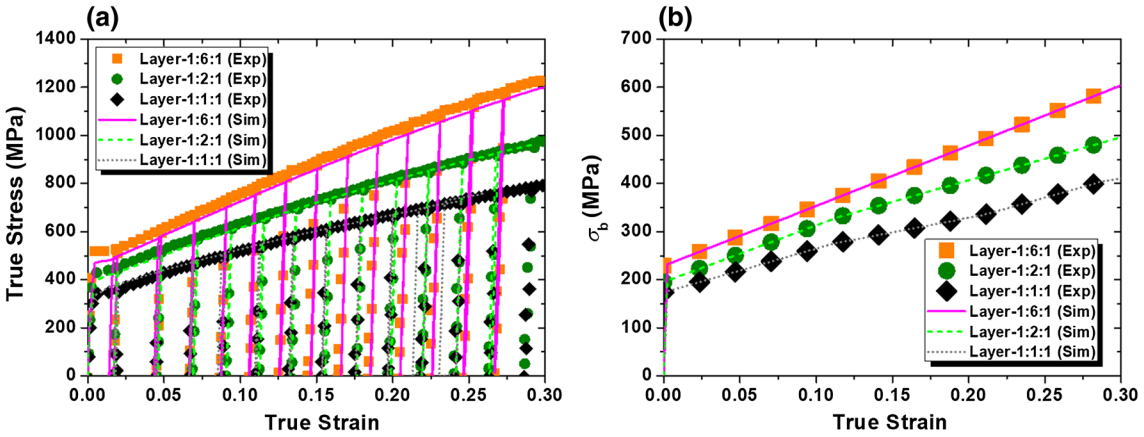

Fig. 5 **a** True stress–strain curves of the TWIP + IF layered steel sheets from the LUR test and from the back-stress-considering FEM simulation. **b** Back-stress (σ_B) evolution of the TWIP + IF layered steels

from σ_B evolution at the TWIP-IF interface. Although the stress–strain curves are well correlated with the non-linear combined isotropic and kinematic hardening FEM results, the accuracy of the kinematic hardening cannot be proven simply by using monotonic uniaxial tensile tests. To evaluate the accuracy of the kinematic hardening behavior in the non-linear combined isotropic and kinematic hardening FEM code, the FEM simulation was also conducted using the LUR test conditions. Figure 5a presents the true stress–strain curves of the TWIP + IF layered steel sheets from the LUR tests, and this time, the stress–strain curves from the non-linear combined isotropic and kinematic hardening FEM well match the experimental results. Moreover, the σ_B calculated from each hysteresis loop shows that the σ_B estimated in the FEM simulation is correlated to the experimental results (Fig. 3b) that were the input data for this simulation work. These results prove that the kinematic hardening in the non-linear combined isotropic and kinematic hardening FEM code is not only valid for the monotonic uniaxial tension condition, but is also effective for the complex tension–compression mode.

In summary, the σ_B effect on the mechanical properties of TWIP + IF layered steel sheet was evaluated by conducting both uniaxial tensile and LUR tests. The measured strength of the TWIP + IF layered steel sheet was greater than the strength estimated using the simple ROM, due to extra-strengthening from the accumulation of GNDs. Because the accumulated GNDs consequently produce long-range σ_B [17], the σ_B of TWIP + IF layered steel sheet increases with increase of the plastic strain during the LUR test. The non-linear combined isotropic and kinematic hardening FEM result supports the assertion that σ_B of the TWIP + IF layered steel sheet provides extra-strengthening, while the conventional FEM result shows a deviation from the experimental results. Because the present model considers σ_B by implementing experimental values of it, the detailed relationship between σ_B and strength should be explained using a reasonable constitutive model in the near future.

4 Conclusions

In this study, the σ_B effect on the mechanical property of TWIP + IF layered steel was evaluated by conducting experimental and simulation work in order to explain that the strength of the layered steel sheet is greater than the value estimated using the simple ROM. The non-linear combined isotropic and kinematic hardening simulation supports the notion that the strength of the layered steel sheet can be enhanced by σ_B. Moreover, the conventional FEM result could not explain the deviation from the experimental result. Therefore, σ_B contributes to the strength enhancement of HS materials and a kinematic hardening term should be added to consider the σ_B effect for more accurate simulation of HS materials.

Acknowledgements This work was supported by the National Research Foundation of Korea (NRF) grant funded by the Ministry of Science, ICT and Future Planning (MSIP) of Korea (NRF-2017R1A2A1A17069427). Also, this study was supported by the Brain Korea 21 PLUS project for Center for Creative Industrial Materials (F16SN25D1706).

References

1. X. Wu, Y. Zhu, Mater. Res. Lett. **5**, 1 (2017)
2. Y. Wei, Y. Li, L. Zhu, Y. Liu, X. Lei, G. Wang, Y. Wu, X. Mi, J. Liu, H. Wang, H. Gao, Nat. Commun. **5**, 3580 (2014)
3. C. Ye, A. Telang, A.S. Gill, S. Suslov, Y. Idell, K. Zweiacker, J.M.K. Wiezorek, Z. Zhou, D. Qian, S.R. Mannava, V.K. Vasudevan, Mater. Sci. Eng. A **613**, 274 (2014)

4. K.-G. Chin, C.Y. Kang, J. Park, S. Lee, Met. Mater. Int. **24**, 489 (2018)
5. H. Springer, C.C. Tasan, D. Raabe, Int. J. Mater. Res. **106**, 3 (2014)
6. R. Zheng, Z. Zhang, M. Nakatani, M. Ota, X. Chen, C. Ma, K. Ameyama, Mater. Sci. Eng. A **674**, 212 (2016)
7. X. Ma, C. Huang, J. Moering, M. Ruppert, H.W. Höppel, M. Göken, J. Narayan, Y. Zhu, Acta Mater. **116**, 43 (2016)
8. J.G. Kim, S.M. Baek, H.H. Lee, K.-G. Chin, S. Lee, H.S. Kim, Acta Mater. **147**, 304 (2018)
9. D.H. Lee, J.-S. Kim, H. Song, S. Lee, Met. Mater. Int. **23**, 805 (2017)
10. S.K. Vajpai, M. Ota, Z. Zhang, K. Ameyama, Mater. Res. Lett. **4**, 1 (2016)
11. H.K. Park, K. Ameyama, J. Yoo, H. Hwang, H.S. Kim, Mater. Res. Lett. **6**, 261 (2018)
12. X. Liu, F. Yuan, Y. Zhu, X. Wu, Scr. Mater. **150**, 57 (2018)
13. X. Wu, P. Jiang, L. Chen, F. Yuan, Y.T. Zhu, Proc. Natl. Acad. Sci. USA **111**, 7197 (2014)
14. X.L. Wu, P. Jiang, L. Chen, J.F. Zhang, F.P. Yuan, Y.T. Zhu, Mater. Res. Lett. **2**, 185 (2014)
15. M. Yang, Y. Pan, F. Yuan, Y. Zhu, X. Wu, Mater. Res. Lett. **4**, 145 (2016)
16. M. Calcagnotto, D. Ponge, E. Demir, D. Raabe, Mater. Sci. Eng. A **527**, 2738 (2010)
17. L. Zhonghua, G. Haicheng, Metall. Trans. A **21**, 717 (1990)
18. X. Wu, M. Yang, F. Yuan, G. Wu, Y. Wei, X. Huang, Y. Zhu, Proc. Natl. Acad. Soc. USA **112**, 14501 (2015)
19. B. Chun, J. Jin, J. Lee, Int. J. Plast **18**, 571 (2002)
20. K. Chen, J.P. Lin, M.K. Lv, L.Y. Wang, Adv. Mater. Res. **97**, 200 (2010)
21. L. Papeleux, J.-P. Ponthot, J. Mater. Process. Technol. **125**, 785 (2002)
22. S. Panthi, N. Ramakrishnan, M. Ahmed, S.S. Singh, M.D. Goel, Mater. Des. **31**, 657 (2010)
23. J.G. Kim, S.M. Baek, J.I. Yoon, M.H. Seo, W.T. Cho, K.-G. Chin, S. Lee, H.S. Kim, J. Mater. Process. Technol. **250**, 357 (2017)
24. J.G. Kim, S.M. Baek, W.T. Cho, T.J. Song, K.-G. Chin, S. Lee, H.S. Kim, Met. Mater. Int. **23**, 459 (2017)